Newtonian Flow in Converging-Diverging Capillaries

Taha Sochi*

April 4, 2012

*Imaging Sciences & Biomedical Engineering, King's College London, The Rayne Institute, St Thomas' Hospital, London, SE1 7EH, UK. Email: taha.sochi@kcl.ac.uk.

Contents

List of Figures

List of Tables

Abstract

The one-dimensional Navier-Stokes equations are used to derive analytical expressions for the relation between pressure and volumetric flow rate in capillaries of five different converging-diverging axisymmetric geometries for Newtonian fluids. The results are compared to previously derived expressions for the same geometries using the lubrication approximation. The results of the one-dimensional Navier-Stokes are identical to those obtained from the lubrication approximation within a non-dimensional numerical factor.

1 Introduction

Modeling the flow through capillaries of converging-diverging geometries is an important subject and has many scientific and industrial applications. Moreover, it is required for modeling viscoelasticity, yield-stress and the flow of Newtonian and non-Newtonian fluids through porous media [1–6].

There are many previous attempts to model the flow through capillaries of various geometries. However, they either apply to tubes of regular cross sections [7, 8] or deal with very special cases. Most these studies use numerical mesh techniques such as finite difference and spectral methods to obtain numerical results. Some examples of these attempts are Kozicki *et al.* [9], Miller [10], Oka [11], Williams and Javadpour [12], Phan-Thien *et al.* [13, 14], Lahbabi and Chang [15], Burdette *et al.* [16], Pilitsis *et al.* [17, 18], James *et al.* [19], Talwar and Khomami [20], Koshiba *et al.* [21], Masuleh and Phillips [22], and Davidson *et al.* [23].

In this article we use the one-dimensional Navier-Stokes equations to derive analytical expressions for the flow of Newtonian fluids in tubes of five axisymmetric converging-diverging geometries, some of which are schematically depicted in Figure 1, and compare our results to previously derived expressions using the lubrication approximation [24].

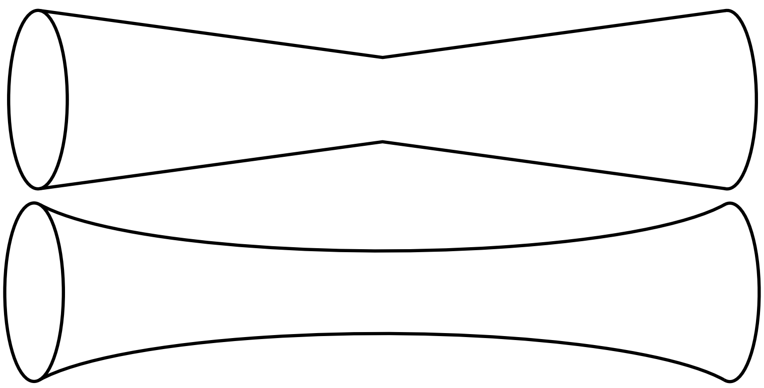

Figure 1: Profiles of converging-diverging axisymmetric capillaries.

The widely-used one-dimensional form of the Navier-Stokes equations to de-

scribe the flow in a tube of length L where its axis is aligned with the x axis and its midpoint is at $x = 0$ is given by the following continuity and momentum balance relations respectively assuming negligible gravitational body forces [25–37]

$$\frac{\partial A}{\partial t} + \frac{\partial Q}{\partial x} = 0 \qquad t > 0, \;\; x \in \left[-\frac{L}{2}, \frac{L}{2}\right] \tag{1}$$

$$\frac{\partial Q}{\partial t} + \frac{\partial}{\partial x}\left(\frac{\alpha Q^2}{A}\right) + \frac{A}{\rho}\frac{\partial p}{\partial x} + \kappa\frac{Q}{A} = 0 \qquad t > 0, \;\; x \in \left[-\frac{L}{2}, \frac{L}{2}\right] \tag{2}$$

In these equations, A is the tube cross sectional area, t is the time, Q $(= A\overline{u})$ is the volumetric flow rate, x is the axial coordinate along the tube, $\alpha (= \frac{\int u^2 dA}{A\overline{u}^2})$ is the momentum flux correction factor, ρ is the fluid mass density, p is the pressure, and κ is a viscosity friction coefficient which is given by $\kappa = \frac{2\pi\alpha\mu}{\rho(\alpha-1)}$ with μ being the fluid dynamic viscosity. For steady flow, the time terms are zero, and hence Q as a function of x is constant. The momentum equation then becomes

$$\frac{\partial}{\partial x}\left(\frac{\alpha Q^2}{A}\right) + \frac{A}{\rho}\frac{\partial p}{\partial x} + \kappa\frac{Q}{A} = 0 \tag{3}$$

that is

$$\frac{\partial p}{\partial x} = -\frac{\rho}{A}\frac{\partial}{\partial x}\left(\frac{\alpha Q^2}{A}\right) - \kappa\rho\frac{Q}{A^2} = \frac{\rho\alpha Q^2}{A^3}\frac{\partial A}{\partial x} - \kappa\rho\frac{Q}{A^2} \tag{4}$$

For a flow in the positive x direction, the pressure gradient is negative and hence

$$p = \int_X \kappa\rho\frac{Q}{A^2}dx - \int_X \frac{\rho\alpha Q^2}{A^3}\frac{\partial A}{\partial x}dx \tag{5}$$

$$= \int_X \kappa\rho\frac{Q}{A^2}dx - \int_A \frac{\rho\alpha Q^2}{A^3}dA \tag{6}$$

$$= \kappa\rho Q \int_X \frac{dx}{A^2} - \rho\alpha Q^2 \int_A \frac{dA}{A^3} \tag{7}$$

that is

$$p = \kappa\rho Q \int_{x=-L/2}^{L/2} \frac{dx}{A^2} + \frac{\rho\alpha Q^2}{2} \left[\frac{1}{A^2}\right]_{x=-L/2}^{L/2} \tag{8}$$

Due to the tube symmetry with respect to $x = 0$

$$\int_{x=-L/2}^{L/2} \frac{dx}{A^2} = 2 \int_{x=0}^{L/2} \frac{dx}{A^2} \tag{9}$$

and

$$\left[\frac{1}{A^2}\right]_{x=-L/2}^{L/2} = 0 \tag{10}$$

Hence

$$p = 2\kappa\rho Q \int_{x=0}^{L/2} \frac{dx}{A^2} \tag{11}$$

This expression is dimensionally consistent.

1.1 Conical Tube

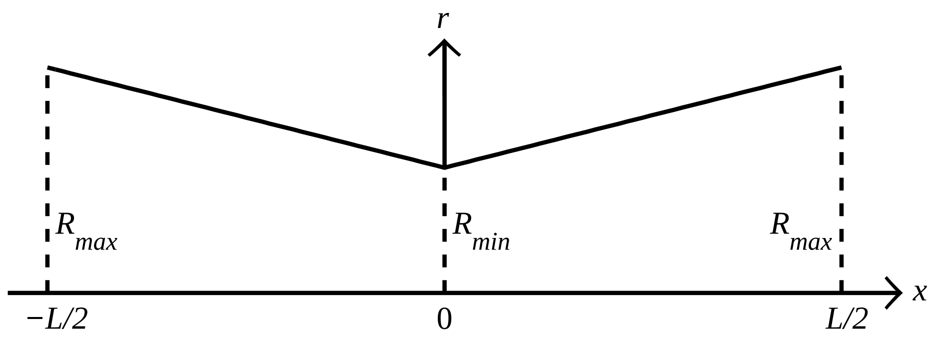

Figure 2: Schematic representation of the radius of a conically shaped converging-diverging capillary as a function of the distance along the tube axis.

For a tube of a conical profile, depicted in Figure 2, the radius r as a function of the axial distance x is given by

$$r(x) = a + b|x| \qquad -L/2 \leq x \leq L/2 \tag{12}$$

where

$$a = R_{min} \qquad \text{and} \qquad b = \frac{2(R_{max} - R_{min})}{L} \tag{13}$$

Hence, Equation 11 becomes

$$p = 2\kappa\rho Q \int_{x=0}^{L/2} \frac{dx}{A^2} = 2\kappa\rho Q \int_{x=0}^{L/2} \frac{dx}{\pi^2 (a + bx)^4} \tag{14}$$

$$= -2\kappa\rho Q \left[\frac{1}{3\pi^2 b (a + bx)^3} \right]_0^{L/2} \tag{15}$$

$$= -2\kappa\rho Q \left[\frac{1}{3\pi^2 \frac{2(R_{max}-R_{min})}{L} \left(R_{min} + \frac{2(R_{max}-R_{min})}{L} x \right)^3} \right]_0^{L/2} \tag{16}$$

$$= -2\kappa\rho Q \left[\frac{L}{6\pi^2 (R_{max} - R_{min}) R_{max}^3} - \frac{L}{6\pi^2 (R_{max} - R_{min}) R_{min}^3} \right] \tag{17}$$

that is

$$p = \frac{\kappa\rho Q L}{3\pi^2 (R_{max} - R_{min})} \left[\frac{1}{R_{min}^3} - \frac{1}{R_{max}^3} \right] \tag{18}$$

1.2 Parabolic Tube

For a tube of parabolic profile, depicted in Figure 3, the radius is given by

$$r(x) = a + bx^2 \qquad -L/2 \leq x \leq L/2 \tag{19}$$

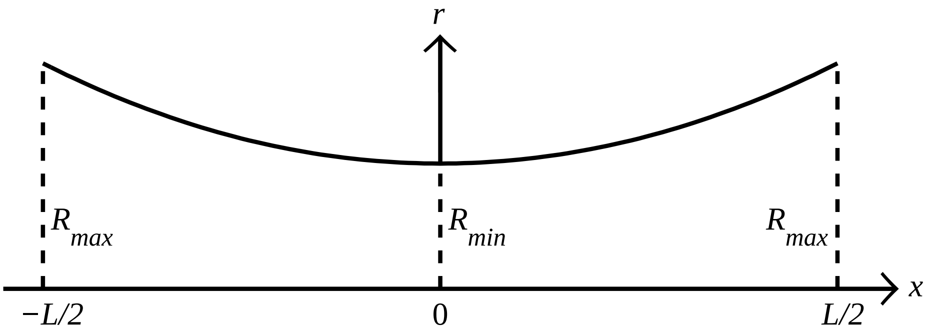

Figure 3: Schematic representation of the radius of a converging-diverging capillary with a parabolic profile as a function of the distance along the tube axis.

where

$$a = R_{min} \qquad \text{and} \qquad b = \left(\frac{2}{L}\right)^2 (R_{max} - R_{min}) \tag{20}$$

Therefore, Equation 11 becomes

$$p = 2\kappa\rho Q \int_{x=0}^{L/2} \frac{dx}{A^2} = 2\kappa\rho Q \int_{x=0}^{L/2} \frac{dx}{\pi^2 (a + bx^2)^4} \tag{21}$$

$$= \frac{2\kappa\rho Q}{\pi^2} \left[\frac{x}{6a (a + bx^2)^3} + \frac{5x}{24a^2 (a + bx^2)^2} + \frac{5x}{16a^3 (a + bx^2)} + \frac{5 \arctan\left(x\sqrt{\frac{b}{a}}\right)}{16a^{7/2}\sqrt{b}} \right]_0^{L/2} \tag{22}$$

that is

$$p = \frac{\kappa\rho Q L}{2\pi^2} \left[\frac{1}{3R_{min}R_{max}^3} + \frac{5}{12R_{min}^2 R_{max}^2} + \frac{5}{8R_{min}^3 R_{max}} + \frac{5 \arctan\left(\sqrt{\frac{R_{max}-R_{min}}{R_{min}}}\right)}{8R_{min}^{7/2}\sqrt{R_{max} - R_{min}}} \right] \tag{23}$$

1.3 Hyperbolic Tube

For a tube of hyperbolic profile, similar to the profile in Figure 3, the radius is given by

$$r(x) = \sqrt{a + bx^2} \qquad -L/2 \le x \le L/2 \qquad a, b > 0 \tag{24}$$

where

$$a = R_{min}^2 \qquad \text{and} \qquad b = \left(\frac{2}{L}\right)^2 (R_{max}^2 - R_{min}^2) \tag{25}$$

Therefore, Equation 11 becomes

$$p = 2\kappa\rho Q \int_{x=0}^{L/2} \frac{dx}{A^2} = 2\kappa\rho Q \int_{x=0}^{L/2} \frac{dx}{\pi^2 \left(a + bx^2\right)^2} \tag{26}$$

$$= \frac{2\kappa\rho Q}{\pi^2} \left[\frac{x}{2a(a + bx^2)} + \frac{\arctan(x\sqrt{b/a})}{2a\sqrt{ab}} \right]_0^{L/2} \tag{27}$$

that is

$$p = \frac{\kappa\rho Q L}{2\pi^2} \left[\frac{1}{R_{min}^2 R_{max}^2} + \frac{\arctan\left(\sqrt{\frac{R_{max}^2 - R_{min}^2}{R_{min}^2}}\right)}{R_{min}^3 \sqrt{R_{max}^2 - R_{min}^2}} \right] \tag{28}$$

1.4 Hyperbolic Cosine Tube

For a tube of hyperbolic cosine profile, similar to the profile in Figure 3, the radius is given by

$$r(x) = a\cosh(bx) \qquad -L/2 \le x \le L/2 \tag{29}$$

where

$$a = R_{min} \qquad \text{and} \qquad b = \frac{2}{L}\text{arccosh}\left(\frac{R_{max}}{R_{min}}\right) \tag{30}$$

Hence, Equation 11 becomes

$$p = 2\kappa\rho Q \int_{x=0}^{L/2} \frac{dx}{A^2} = 2\kappa\rho Q \int_{x=0}^{L/2} \frac{dx}{\pi^2 a^4 \cosh^4(bx)} \tag{31}$$

$$= \frac{2\kappa\rho Q}{\pi^2}\left[\frac{\tanh(bx)\left[\text{sech}^2(bx)+2\right]}{3a^4 b}\right]_0^{L/2} \tag{32}$$

that is

$$p = \frac{\kappa\rho Q L}{3\pi^2}\left[\frac{\tanh\left(\text{arccosh}\left(\frac{R_{max}}{R_{min}}\right)\right)\left[\text{sech}^2\left(\text{arccosh}\left(\frac{R_{max}}{R_{min}}\right)\right)+2\right]}{R_{min}^4 \quad \text{arccosh}\left(\frac{R_{max}}{R_{min}}\right)}\right] \tag{33}$$

1.5 Sinusoidal Tube

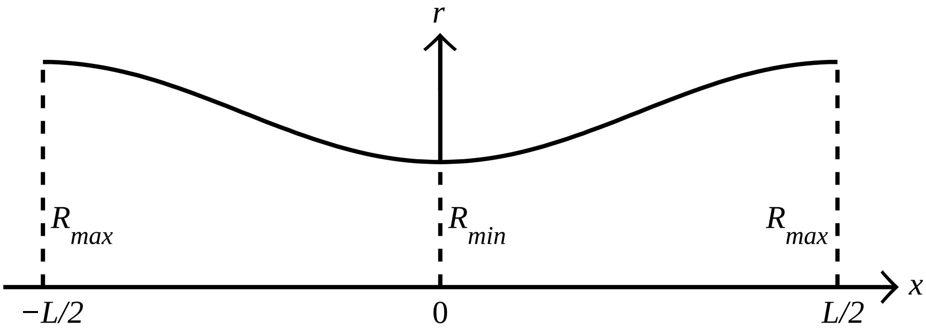

Figure 4: Schematic representation of the radius of a converging-diverging capillary with a sinusoidal profile as a function of the distance along the tube axis.

For a tube of sinusoidal profile, depicted in Figure 4, where the tube length L spans one complete wavelength, the radius is given by

$$r(x) = a - b\cos(kx) \qquad -L/2 \le x \le L/2 \qquad a > b > 0 \tag{34}$$

where

$$a = \frac{R_{max} + R_{min}}{2} \qquad b = \frac{R_{max} - R_{min}}{2} \qquad \& \qquad k = \frac{2\pi}{L} \tag{35}$$

Hence, Equation 11 becomes

$$p = 2\kappa\rho Q \int_{x=0}^{L/2} \frac{dx}{A^2} = 2\kappa\rho Q \int_{x=0}^{L/2} \frac{dx}{\pi^2 \left[a - b\cos(kx)\right]^4} \tag{36}$$

On performing this integration, the following relation is obtained

$$p = \frac{2\kappa\rho Q}{\pi^2 b^4 k} \left[I\right]_0^{L/2} \tag{37}$$

where

$$I = \frac{(6B^3 + 9B)}{3(B^2-1)^{7/2}} \arctan\left(\frac{(B-1)\tan(\frac{kx}{2})}{\sqrt{B^2-1}}\right) - \frac{(11B^2+4)\sin(kx)}{6(B^2-1)^3[B+\cos(kx)]} \tag{38}$$

$$-\frac{5B\sin(kx)}{6(B^2-1)^2[B+\cos(kx)]^2} - \frac{\sin(kx)}{3(B^2-1)[B+\cos(kx)]^3} \tag{39}$$

$$\& \qquad B = \frac{R_{max} + R_{min}}{R_{min} - R_{max}} \tag{40}$$

On taking $\lim_{x \to \frac{L}{2}^-} I$ the following expression is obtained

$$p = \frac{2\kappa\rho Q}{\pi^2 b^4 k}\left[-\frac{(6B^3+9B)}{3(B^2-1)^{7/2}}\frac{\pi}{2}\right] = -\frac{\kappa\rho Q(6B^3+9B)}{3\pi b^4 k (B^2-1)^{7/2}} \tag{41}$$

Since $B < -1$, $p > 0$ as it should be. On substituting for B, b and k in the last expression we obtain

$$p = \frac{\kappa\rho Q L\left(R_{max} - R_{min}\right)^3 \left[2\left(\frac{R_{max}+R_{min}}{R_{max}-R_{min}}\right)^3 + 3\left(\frac{R_{max}+R_{min}}{R_{max}-R_{min}}\right)\right]}{16\pi^2 \left(R_{max}R_{min}\right)^{7/2}} \tag{42}$$

It is noteworthy that all these relations (i.e. Equations 18, 23, 28, 33 and 42), are dimensionally consistent. Moreover, they are identical to the lubrication approximation formula (refer to Table 1) for $\alpha = 4/3$.

Table 1: Lubrication approximation table. These formulae are derived in [24].

Conical	$p = \frac{8LQ\mu}{3\pi(R_{max}-R_{min})}\left(\frac{1}{R_{min}^3}-\frac{1}{R_{max}^3}\right)$
Parabolic	$p = \frac{4LQ\mu}{\pi}\left(\frac{1}{3R_{min}R_{max}^3}+\frac{5}{12R_{min}^2R_{max}^2}+\frac{5}{8R_{min}^3R_{max}}+\frac{5\arctan\left(\sqrt{\frac{R_{max}-R_{min}}{R_{min}}}\right)}{8R_{min}^{7/2}\sqrt{R_{max}-R_{min}}}\right)$
Hyperbolic	$p = \frac{4LQ\mu}{\pi}\left(\frac{1}{R_{min}^2R_{max}^2}+\frac{\arctan\left(\sqrt{\frac{R_{max}^2-R_{min}^2}{R_{min}^2}}\right)}{R_{min}^3\sqrt{R_{max}^2-R_{min}^2}}\right)$
Hyperbolic Cosine	$p = \frac{8LQ\mu}{3\pi R_{min}^4}\left(\frac{\tanh\left(\text{arccosh}\left(\frac{R_{max}}{R_{min}}\right)\right)\left\{\text{sech}^2\left(\text{arccosh}\left(\frac{R_{max}}{R_{min}}\right)\right)+2\right\}}{\text{arccosh}\left(\frac{R_{max}}{R_{min}}\right)}\right)$
Sinusoidal	$p = \frac{LQ\mu\left\{2(R_{max}+R_{min})^3+3(R_{max}+R_{min})(R_{max}-R_{min})^2\right\}}{2\pi(R_{max}R_{min})^{7/2}}$

2 Conclusions

In this paper we derived analytical expressions relating the pressure drop to the volumetric flow rate for Newtonian fluids in five different converging-diverging geometries using the one-dimensional Navier-Stokes flow equations in axisymmetric tubes. The results obtained in this paper are identical, within a non-dimensional numerical factor, to those derived in [24] using the lubrication approximation. These expressions can be used in various practical scientific and engineering situations to describe isothermal, uniform, laminar flow of incompressible, time-independent Newtonian fluids. These situations include the flow in corrugated vessels and the flow in the pores and throats of porous media where the converging-diverging nature can be idealized by one of these simple geometries. The analytical method can also be used to derive expressions for axisymmetric geometries other than those presented in this paper.

Nomenclature

α	correction factor for axial momentum flux
κ	viscosity friction coefficient ($m^2.s^{-1}$)
μ	fluid dynamic viscosity (Pa.s)
ρ	fluid mass density ($kg.m^{-3}$)
A	tube cross sectional area (m^2)
L	tube length (m)
p	pressure (Pa)
Q	volumetric flow rate ($m^3.s^{-1}$)
r	tube radius (m)
R_{max}	maximum radius of converging-diverging tube (m)
R_{min}	minimum radius of converging-diverging tube (m)
t	time (s)
u	local axial fluid speed ($m.s^{-1}$)
$\overline{u}$	mean axial fluid speed ($m.s^{-1}$)
x	axial coordinate (m)

References

[1] T. Sochi; M.J. Blunt. Pore-scale network modeling of Ellis and Herschel-Bulkley fluids. *Journal of Petroleum Science and Engineering*, 60(2):105–124, 2008. 5

[2] T. Sochi. Pore-scale modeling of viscoelastic flow in porous media using a Bautista-Manero fluid. *International Journal of Heat and Fluid Flow*, 30(6):1202–1217, 2009. 5

[3] T. Sochi. Non-Newtonian Flow in Porous Media. *Polymer*, 51(22):5007–5023, 2010. 5

[4] T. Sochi. Modelling the Flow of Yield-Stress Fluids in Porous Media. *Transport in Porous Media*, 85(2):489–503, 2010. 5

[5] T. Sochi. Computational Techniques for Modeling Non-Newtonian Flow in Porous Media. *International Journal of Modeling, Simulation, and Scientific Computing*, 1(2):239–256, 2010. 5

[6] T. Sochi. Flow of Non-Newtonian Fluids in Porous Media. *Journal of Polymer Science Part B*, 2010. 5

[7] F.M. White. *Viscous Fluid Flow*. McGraw Hill Inc., second edition, 1991. 5

[8] S. Sisavath; X. Jing; R.W. Zimmerman. Laminar Flow Through Irregularly-Shaped Pores in Sedimentary Rocks. *Transport in Porous Media*, 45(1):41–62, 2001. 5

[9] W. Kozicki; C.H. Chou; C. Tiu. Non-Newtonian flow in ducts of arbitrary cross-sectional shape. *Chemical Engineering Science*, 21(8):665–679, 1966. 5

[10] C. Miller. Predicting Non-Newtonian Flow Behavior in Ducts of Unusual Cross Section. *Industrial & Engineering Chemistry Fundamentals*, 11(4):524–528, 1972. 5

[11] S. Oka. Pressure development in a non-Newtonian flow through a tapered tube. *Rheologica Acta*, 12(2):224–227, 1973. 5

[12] E.W. Williams; S.H. Javadpour. The flow of an elastico-viscous liquid in an axisymmetric pipe of slowly varying cross-section. *Journal of Non-Newtonian Fluid Mechanics*, 7(2-3):171–188, 1980. 5

[13] N. Phan-Thien; C.J. Goh; M.B. Bush. Viscous flow through corrugated tube by boundary element method. *Journal of Applied Mathematics and Physics (ZAMP)*, 36(3):475–480, 1985. 5

[14] N. Phan-Thien; M.M.K. Khan. Flow of an Oldroyd-type fluid through a sinusoidally corrugated tube. *Journal of Non-Newtonian Fluid Mechanics*, 24(2):203–220, 1987. 5

[15] A. Lahbabi; H-C Chang. Flow in periodically constricted tubes: Transition to inertial and nonsteady flows. *Chemical Engineering Science*, 41(10):2487–2505, 1986. 5

[16] S.R. Burdette; P.J. Coates; R.C. Armstrong; R.A. Brown. Calculations of viscoelastic flow through an axisymmetric corrugated tube using the explicitly elliptic momentum equation formulation (EEME). *Journal of Non-Newtonian Fluid Mechanics*, 33(1):1–23, 1989. 5

[17] S. Pilitsis; A. Souvaliotis; A.N. Beris. Viscoelastic flow in a periodically constricted tube: The combined effect of inertia, shear thinning, and elasticity. *Journal of Rheology*, 35(4):605–646, 1991. 5

[18] S. Pilitsis; A.N. Beris. Calculations of steady-state viscoelastic flow in an undulating tube. *Journal of Non-Newtonian Fluid Mechanics*, 31(3):231–287, 1989. 5

[19] D.F. James; N. Phan-Thien; M.M.K. Khan; A.N. Beris; S. Pilitsis. Flow of test fluid M1 in corrugated tubes. *Journal of Non-Newtonian Fluid Mechanics*, 35(2-3):405–412, 1990. 5

[20] K.K. Talwar; B. Khomami. Application of higher order finite element methods to viscoelastic flow in porous media. *Journal of Rheology*, 36(7):1377–1416, 1992. 5

[21] T. Koshiba; N. Mori; K. Nakamura; S. Sugiyama. Measurement of pressure loss and observation of the flow field in viscoelastic flow through an undulating channel. *Journal of Rheology*, 44(1):65–78, 2000. 5

[22] S.H. Momeni-Masuleh; T.N. Phillips. Viscoelastic flow in an undulating tube using spectral methods. *Computers & fluids*, 33(8):1075–1095, 2004. 5

[23] D. Davidson; G.L. Lehmann; E.J. Cotts. Horizontal capillary flow of a Newtonian liquid in a narrow gap between a plane wall and a sinusoidal wall. *Fluid Dynamics Research*, 40(11-12):779–802, 2008. 5

[24] T. Sochi. The Flow of Newtonian Fluids in Axisymmetric Corrugated Tubes. 2010. arXiv:1006.1515v1. 5, 13, 14

[25] L. Formaggia; J.F. Gerbeau; F. Nobile; A. Quarteroni. On the coupling of 3D and 1D Navier-Stokes equations for flow problems in compliant vessels. *Computer Methods in Applied Mechanics and Engineering*, 191(6-7):561–582, 2001. 6

[26] W. Ruan; M.E. Clark; M. Zhao; A. Curcio. A Hyperbolic System of Equations

of Blood Flow in an Arterial Network. *SIAM Journal on Applied Mathematics*, 64(2):637–667, 2003. 6

[27] S.J. Sherwin; V. Franke; J. Peiró; K. Parker. One-dimensional modelling of a vascular network in space-time variables. *Journal of Engineering Mathematics*, 47(3-4):217–250, 2003. 6

[28] S. Urquiza; P. Blanco; G. Lombera; M. Venere; R. Feijoo. Coupling Multidimensional Compliant Models For Carotid Artery Blood Flow. *Mecánica Computacional*, XXII(3):232–243, 2003. 6

[29] V. Milišić; A. Quarteroni. Analysis of lumped parameter models for blood flow simulations and their relation with 1D models. *Mathematical Modelling and Numerical Analysis*, 38(4):613–632, 2004. 6

[30] M.Á. Fernández; V. Milišić; A. Quarteroni. Analysis of a Geometrical Multiscale Blood Flow Model Based on the Coupling of ODEs and Hyperbolic PDEs. *Multiscale Modeling & Simulation*, 4(1):215–236, 2005. 6

[31] L. Formaggia; D. Lamponi; M. Tuveri; A. Veneziani. Numerical modeling of 1D arterial networks coupled with a lumped parameters description of the heart. *Computer Methods in Biomechanics and Biomedical Engineering*, 9(5):273–288, 2006. 6

[32] L. Formaggia; A. Moura; F. Nobile. Coupling 3D and 1D fluid-structure interaction models for blood flow simulations. *Proceedings in Applied Mathematics and Mechanics, Special Issue: GAMM Annual Meeting 2006 - Berlin*, 6(1):27–30, 2006. 6

[33] J. Alastruey; S.M. Moore; K.H. Parker; T. David; J. Peiró S.J. Sherwin. Reduced modelling of blood flow in the cerebral circulation: Coupling 1-D,

0-D and cerebral auto-regulation models. *International Journal for Numerical Methods in Fluids*, 56(8):1061–1067, 2008. 6

[34] J. Alastruey; K.H. Parker; J. Peiró; S.J. Sherwin. Lumped parameter outflow models for 1-D blood flow simulations: Effect on pulse waves and parameter estimation. *Communications in Computational Physics*, 4(2):317–336, 2008. 6

[35] J. Lee; N. Smith. Development and application of a one-dimensional blood flow model for microvascular networks. *Proceedings of the Institution of Mechanical Engineers, Part H: Journal of Engineering in Medicine*, 222(4):487–512, 2008. 6

[36] T. Passerini; M. de Luca; L. Formaggia; A. Quarteroni; A. Veneziani. A 3D/1D geometrical multiscale model of cerebral vasculature. *Journal of Engineering Mathematics*, 64(4):319–330, 2009. 6

[37] J. Janela; A.B. de Moura; A. Sequeira. Comparing Absorbing Boundary Conditions for a 3D Non Newtonian Fluid-Structure Interaction Model for Blood Flow in Arteries. *Mecánica Computacional*, XXIX(59):5961–5971, 2010. 6